NJC

PAPER

Cite this: *New J. Chem.*, 2017, **41**, 12685

Experimental and computational investigation of the substituent effects on the reduction of Fe^{3+} by 1,2-dihydroxybenzenes†

Pablo Salgado,[a] David Contreras,[bc] Héctor D. Mansilla,[b] Katherine Márquez,[c] Gladys Vidal,[a] Carlos J. Cobos[d] and Daniel O. Mártire *[d]

Received 20th April 2017,
Accepted 11th September 2017

DOI: 10.1039/c7nj01322a

rsc.li/njc

This study reports on the kinetics of the early steps that mediate the reactions of substituted 1,2-dihydroxybenzenes (1,2-DHB) with Fe^{3+}. The rate constants of the three processes identified by means of the stopped-flow technique are affected by the electron-withdrawing or electron-donating abilities of the substituent. The fastest process is assigned to the formation of a 1 : 1 complex between Fe^{3+} and the 1,2-DHB, which is accompanied by proton loss. The second process involves the inner-sphere electron transfer from the ligand to Fe^{3+} and the slowest step is related to the deprotonation of one of the oxygen atoms bonded to the metal. A reaction mechanism is proposed on the basis of the experimental data and density functional theory (DFT) calculations on mono- and bidentate species with different degrees of protonation.

1. Introduction

Siderophores are ferric ion-specific chelating compounds produced by bacteria and fungi growing under the limited availability of iron. They are low molecular weight compounds (600–1500 Daltons), which chelate ferric iron with an extremely high affinity, and the complex is actively transported for instance across the outer and inner membranes of Gram-negative bacteria.[1] There are two main classes of siderophores: catechols and hydroxamates. Catechol-type siderophores chelate ferric iron *via* hydroxyl groups, and hydroxamate-type siderophores chelate ferric iron *via* a carbonyl group with an adjacent nitrogen. After complexation only catechol-type siderophores can reduce Fe^{3+} to Fe^{2+} at acidic pH.[2,3]

In the microorganisms present in some plants, such as rot fungi, it was shown that oxalic acid is produced for sequestration of Fe^{3+} and lowering of pH in a region close to the hyphae.[4] These rot fungi are also able to produce catechol-type ligands, which uptake the Fe^{3+} sequestered by oxalic acid and reduce it to Fe^{2+}. These ions further react with enzymatically produced H_2O_2[5,6] to yield $^{\bullet}OH$ radicals (Fenton reaction), which degrade the wood and the byproducts generated are taken up by the fungi.[7,8] In addition, some neurodegenerative diseases, such as Alzheimer and Parkinson, are related to the presence of Fe^{3+} and catecholamines like dopamine, epinephrine, and norepinephrine,[9–11] highlighting the relevance of understanding the interactions between catechol-like ligands and Fe^{3+}.

Much effort has been devoted to study the process of Fe^{3+} reduction by polyphenols. The model compounds most investigated were catechol derivatives.[12–16] Several mechanisms have been proposed in the literature to account for the Fe^{3+} reduction by 1,2-dihydroxybenzene (1,2-DHB). The most accepted mechanism is shown in Scheme 1. In the first reaction step the catechol forms a 1 : 1 complex with Fe^{3+} (species I). This type of bidentate complex was proposed by Hider *et al.*[17] for catechol and by Kristinová *et al.*[15] for three carboxylic acids derived from catechol: caffeic, ferulic, *p*-coumaric acids. The complexes further suffer deprotonation to yield species II. This process is followed by an inner-sphere electron transfer from ligand to metal leading to formation of the semiquinone–Fe^{2+} complex, *i.e.*, a hydroxyphenoxyl radical (species IV), as proposed by Kristinová *et al.* for the carboxylic acids and by Hynes and O'Coinceanainn.[18] The reaction then proceeds again by deprotonation to yield an *ortho*-semiquinone radical V.[18] This reactive radical finally loses Fe^{2+} leading to species VII and is oxidized either by Fe^{3+}[15,18] or oxygen in one or more steps[15] to yield the biradical VIII, in equilibrium with quinone IX.

A reaction intermediate with an absorption maximum at around 700 nm was detected and assigned by some authors to

[a] *Grupo de Ingeniería y Biotecnología Ambiental, Facultad de Ciencias Ambientales y Centro EULA-Chile, Universidad de Concepción, Casilla 160-C, Concepción, Chile*
[b] *Facultad de Ciencias Químicas, Universidad de Concepción, Casilla 160-C, Concepción, Chile*
[c] *Centro de Biotecnología, Universidad de Concepción, Concepción, Chile*
[d] *Instituto de Investigaciones Fisicoquímicas Teóricas y Aplicadas (INIFTA), Facultad de Ciencias Químicas, Universidad Nacional de la Plata, CONICET, Casilla de Correo 16, Sucursal 4, 1900 La Plata, Argentina. E-mail: dmartire@inifta.unlp.edu.ar*

† Electronic supplementary information (ESI) available. See DOI: 10.1039/c7nj01322a

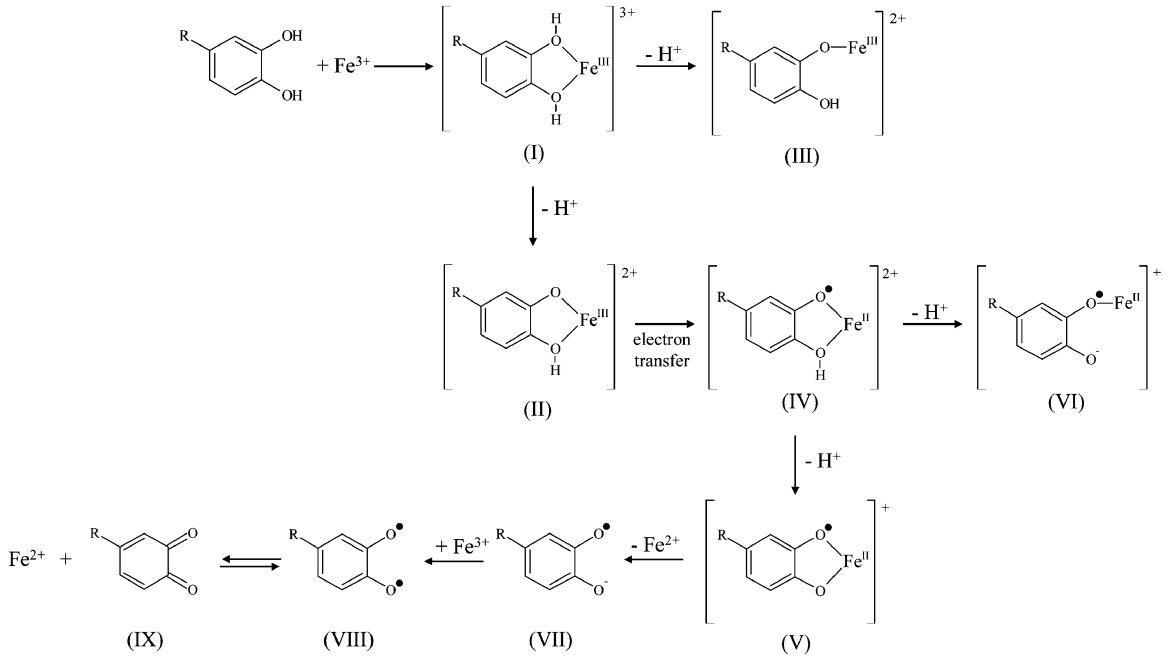

Scheme 1 Proposed mechanism for the reduction of Fe^{3+} by 1,2-DHB.

species II[15,18–20] and by others to species IV.[17,19,21] Although not considered in the literature, deprotonation of species I could lead to a monodentate complex of Fe^{3+} (species III). Similarly, the monodentate complex between Fe^{2+} and the semiquinone (species VI) could be formed upon deprotonation of species IV.

The stability constants of the complexes of transition metals with 4-substituted catechols were shown to depend on the electron withdrawing ability of the substituent.[22] In particular, Nurchi *et al.*[23] investigated the equilibria of iron(III) with catechol and its 4-nitro derivative by potentiometry, spectrophotometry, and NMR spectroscopy. These authors found that the inductive and resonance properties of the nitro substituent led to a general decrease in the complex formation constants. This background motivated us to make a systematic study of the substituent effect of the reaction between 4-substituted catechols and Fe^{3+} in acid medium. To this purpose we obtained kinetic and spectroscopic information on these reactions by means of the stopped-flow technique. A reaction mechanism is proposed with the aid of the effect of the electron-withdrawing ability of the substituent on the rate constants of the three observed processes. Density functional theory (DFT) calculations of molecular structures, vibrational frequencies, thermodynamic properties and absorption spectra of the relevant species proposed in the reaction mechanism helped us to understand the participation in the reaction mechanism of mono- and bidentate species with different protonation degrees.

2. Experimental

2.1 Materials and methods

Catechol, 4-methylcatechol, 4-ethylcatechol, 4-*tert*-butylcatechol, 3,4-dihydroxybenzonitrile and ferric nitrate ($Fe(NO_3)_3{\cdot}9H_2O$) were purchased from Sigma-Aldrich; whereas 3,4-dihydroxybenzoic acid, 3,4-dihydroxybenzaldehyde, 4-nitrocatechol, and nitric acid (HNO_3) were purchased from Merck. All solutions were prepared with deionized water, under an Argon atmosphere. Besides, all reactions were carried out at an ionic strength of 0.50 M KNO_3. The pH of each solution used was adjusted using a 3 Start Thermo Orion pH meter.

2.2 Kinetic studies

A Hi-Tech Scientific SFA-20 Rapid Kinetics stopped-flow accessory was employed. The absorbance was measured with a sensitive detection system used for flash-photolysis experiments.[24] Briefly, the analysis light from a 150 W Xe arc lamp was passed through a monochromator (PTI 1695) and detected by a 1P28 PMT photomultiplier. A 10 mm path length quartz cuvette was employed. Decays typically represented the average of 5 signals and were digitized by and stored in a 100 MHz Rigol DS1102E oscilloscope.

2.3 Quantum-chemical calculations

The equilibrium structures, harmonic vibrational frequencies, total electronic energies, Gibbs free energies and electronic transitions of the radical and radical cation intermediates were calculated at the O3LYP/6-311++G(d,p) level of the DFT.[25] This hybrid three-parameter functional is formed by the local exchange functional OPTX[26] and the well-known correlation functional LYP.[27] Solvent effects were accounted for by using the conductor-like polarizable continuum model, CPCM,[28] with a relative permittivity for water of 78.3553. The time-dependent density functional theory (TD-DFT) was employed to estimate the vertical excitation energy and the oscillator strength *f* for each transition. This last magnitude provides information on the band intensity and depends on electronic, Frank–Condon

and spin factors. Up to forty electronic transitions were required to cover the experimental absorption spectra of the species investigated. The oscillator strength was estimated for II, III, IV, V, VI, VII and VIII species (Scheme 1). Note that species II and IV cannot be distinguished in the calculations because they only differ by an internal charge transfer, *i.e.*, they have the same charge and multiplicity. For all calculations the Gaussian 09 package was employed.[29]

3. Results and discussion

3.1 UV-visible absorption spectra

The substituted 1,2-DHB studied here are shown in Scheme 2.

Solutions of Fe^{3+} containing 1,2-DHB with electron donating substituents (EDS) show immediately after the mixture an absorption band at around 700 nm and an additional band at around 400 nm very likely assigned to the formation of quinones (see Fig. 1a for 4-*tert*-butylcatechol). After 1 minute the absorption band at around 700 nm disappears and the band around 400 nm increases. The absorbance changes observed during the first minute after mixing Fe^{3+} and catechol are also similar (Fig. S1, ESI†). However, in the absorption spectra of mixtures of Fe^{3+} with 1,2-DHB with electron withdrawing substituents (EWS), the absorption bands at around 400 nm and 700 nm almost remain unchanged during the first minute (see Fig. 1b for 3,4-dihydroxybenzonitrile).

To obtain information on the evolution of the fast reactions between Fe^{3+} and 1,2-DHB, the kinetics was studied with the aid of a stopped-flow accessory coupled to a spectrophotometer.

3.2 Stopped-flow experiments

The absorbance changes (ΔA) detected in the stopped-flow assays are relative to the final mixture of the reactants. Two different kinetic profiles were observed. For the 1,2-DHB with EDS and catechol above a certain substituent-dependent wavelength, the typical kinetic profiles show a fast increase in absorbance followed by a slower decay (see Fig. 2a for 4-*tert*-butylcatechol at 720 nm, black line). This behavior can be associated with the formation of an intermediate presenting a higher absorbance than the final products within the first hundreds of microseconds. This species decays in the seconds time-scale. The kinetic profiles at two different wavelengths for 1,2-DHB with EWS in the whole wavelength range and for 1,2-DHB with EDS and catechol at shorter wavelengths show an initial fast decrease of absorbance, followed by an increase and then a slower decay (see Fig. 2a for 4-*tert*-butylcatechol at 500 nm, yellow line and Fig. 2b for 3,4-dihydroxybenzonitrile at 680 nm). The spectral kinetic profiles for all the 1,2-DHB are shown in Fig. S2 (ESI†).

The kinetics profiles in the 300–800 nm wavelength range were adjusted to eqn (1).

$$\Delta A = a_{(\lambda)}(\exp^{-bt}) + c_{(\lambda)}(\exp^{-dt}) + e_{(\lambda)}(\exp^{-ft}) \quad (1)$$

where the pre-exponential factors $a_{(\lambda)}$, $c_{(\lambda)}$, and $e_{(\lambda)}$, are wavelength-dependent and the apparent rate constants b, d, and f are wavelength-independent.

To investigate the substituent effect on the apparent rate constants b, d, and f, the Hammett eqn (2) was used.

$$\log\left(\frac{k_X}{k^\circ}\right) = \rho\sigma \quad (2)$$

where k_X is the rate constant for substituent X and k° is the corresponding rate constant for X = H (catechol in our case). The σ parameters are a measure of the electron-withdrawing ability of the substituent on the aromatic ring. For the 1,2-DHB the σ parameters were obtained by adding reported values in *meta* (σ_m) and *para* (σ_p) position.[30] The reaction constant (ρ) measures the sensitivity of the reaction to the electronic effect. This constant is independent of the substituent.[31]

Fig. 3 shows the Hammett plots for the rate constants b (first process), d (second process), and f (third process).

The slope of the straight line in Fig. 3a, $\rho = 0.036 \pm 0.002$ ($r = 0.970$), indicates a slight substituent effect, being the reaction favored for those 1,2-DHB with EWS. Ishida *et al.*[32] showed that the first pK_a value for substituted catechols correlate with Hammett parameters, and that electron-withdrawing substituents significantly stabilize the monoanionic species of free catechols. Thus, if the same behavior is valid for the Fe^{3+}

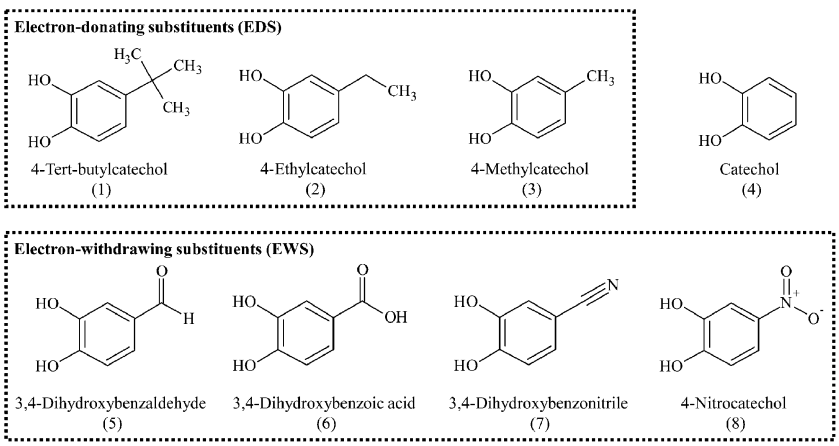

Scheme 2 Structure of the substituted 1,2-DHB investigated in this work.

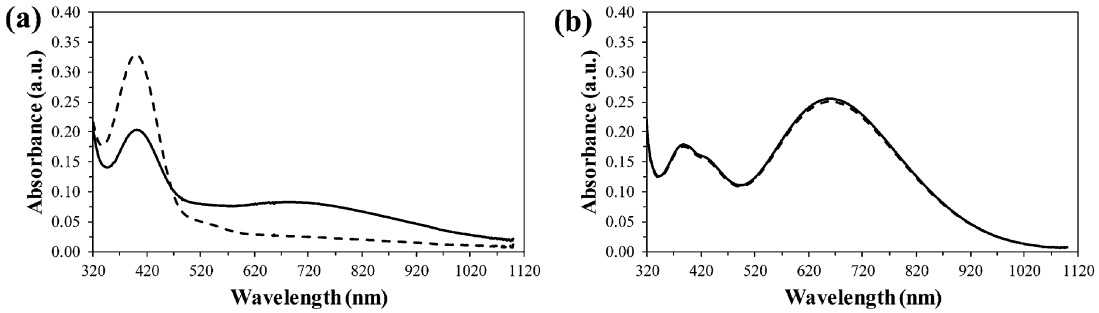

Fig. 1 UV-visible absorption spectra of the mixtures of 1×10^{-4} mol L^{-1} of Fe^{3+} and 1×10^{-2} mol L^{-1} of: (a) 4-*tert*-butylcatechol and (b) 3,4-dihydroxybenzonitrile. Solid lines (—) indicates the UV-visible absorption spectra taken immediately after the mixture and dashed lines (- - -) show the spectra 1 minute after the mixture.

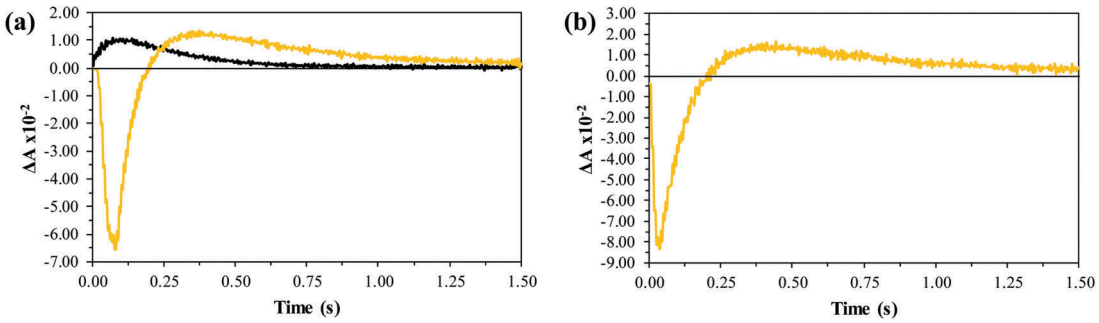

Fig. 2 Kinetic profile obtained for the mixture at pH = 3.0 of 1×10^{-4} mol L^{-1} of Fe^{3+} and 1×10^{-2} mol L^{-1}: (a) 4-*tert*-butylcatechol at 720 nm (black line) and 500 nm (yellow line), (b) 3,4-dihidroxybenzonitrile at 680 nm.

complexes of 1,2-DHB, the first process could be associated with a deprotonation step. Our data seem to indicate that deprotonation either takes place simultaneously with formation of the iron(III) complex or that it is a much faster event.

The slope of the Hammett plot in Fig. 3b is $\rho = -0.15 \pm 0.01$ ($r = 0.975$), which means that the process is sensitive to the substituent and that it is faster for 1,2-DHB with EDS, where the electronic density on the −OH groups is higher. This result

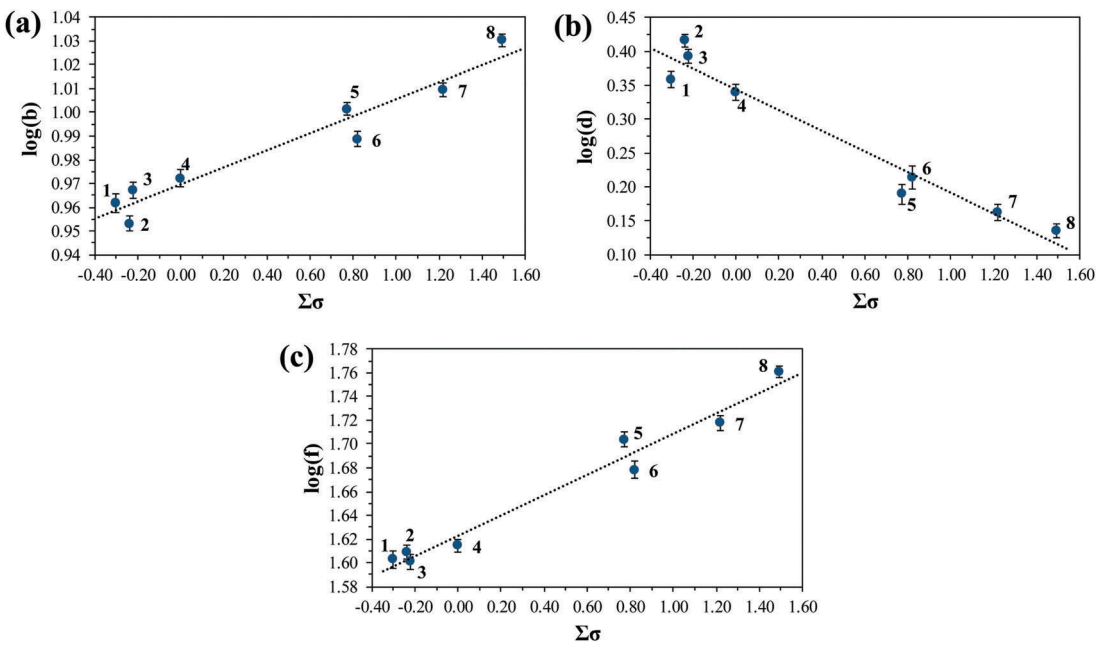

Fig. 3 Hammett plots for rate constants: (a) first process, (b) second process, and (c) third process for 1: 4-*tert*-butylcatechol, 2: 4-ethylcatechol, 3: 4-methylcatechol, 4: catechol, 5: 3,4-dihydroxybenzaldehyde, 6: 3,4-dihydroxybenzoic acid, 7: 3,4-dihydroxybenzonitrile, and 8: 4-nitrocatechol.

makes us assign the process to the intramolecular electron step from (II) to (IV).

From the positive value of the slope of the Hammett plot shown in Fig. 3c for the slowest step, $\rho = 0.085 \pm 0.003$ ($r = 0.985$), we can conclude that this process is moderately favored for 1,2-DHB with EWS. Thus, since the Fe–O bond is expected to be weaker in 1,2-DHB with EWS, the rate-determining step of the slowest process should be the transformation of species (IV) into (VI). This step also involves a deprotonation, and the dependence of its rate on Hammett parameters is in line with that reported by Ishida *et al.*[32] for the first pK_a value of substituted catechols.

According to the previous discussion, the highest concentration of species (II) is expected to be present at the times corresponding to the minimum (t_{min}) or maximum (t_{max}) of those profiles with the shapes of Fig. 2a or b, respectively. The maximum concentration of species (IV) should occur at the t_{max} for those kinetic profiles with the shape of Fig. 2a. Fig. 4 shows the absorbance of species (II) and (IV) relative to the absorption spectra of the final mixtures at the times of their highest concentrations obtained from the kinetic profiles for a typical 1,2-DHB with an EDS substituent (Fig. 4a), catechol (Fig. 4b), and a typical 1,2-DHB with an EWS substituent (Fig. 4c).

3.3 Oscillator strengths of the species involved in the reaction mechanism

To obtain theoretical information related to the experimental absorption spectra the oscillator strengths (f) of several species present in the reaction mechanism were calculated. As mentioned above, species II and IV cannot be distinguished in the calculations. All the calculated oscillator strengths are shown in Table S1, ESI.†

From the theoretical data, it is possible to assign the wavelength region where the species involved in the reaction mechanism mainly absorb. We can observe that species number (VI), (VII), and (VIII), and in a much lesser magnitude species (III) (see Table S2 and Fig. S3, ESI† for the oscillator strengths and wavelengths regions where the species mainly absorb, respectively) absorb above 520 nm. This means that species (VI)–(VIII) are mainly responsible for the absorbance in this wavelength range over the first minute after mixing the reactants (see Fig. 1). It is also observed in Fig. 1 that 1,2-DHB with EWS absorbs more that those with EDS or catechol itself, in excellent agreement with the much higher oscillator strengths calculated for species (VI)–(VIII) of the 1,2-DHB with EWS.

The theoretical data show that the oscillator strengths for species II (or IV) formed with 1,2-DHB containing EDS and catechol are lower than those containing EWS. This result is also in agreement with the experimental data because we should keep in mind that the absorption spectra shown in Fig. 4 are relative to the absorbance of the final mixture.

3.4 Structure of reaction intermediates

Theoretical calculations were performed to investigate whether open (monodentate) or cyclic (bidentate) intermediates are more likely to participate in the reaction mechanism. The optimized geometries of the cyclic and open complexes of Fe^{2+} and Fe^{3+} with 4-methylcatechol are shown in Fig. 5. From the difference in Gibbs free energies between the cyclic and open forms of the complexes (see Table 1) we conclude that monodentate Fe^{3+} complexes are clearly more stable than the bidentate ones,

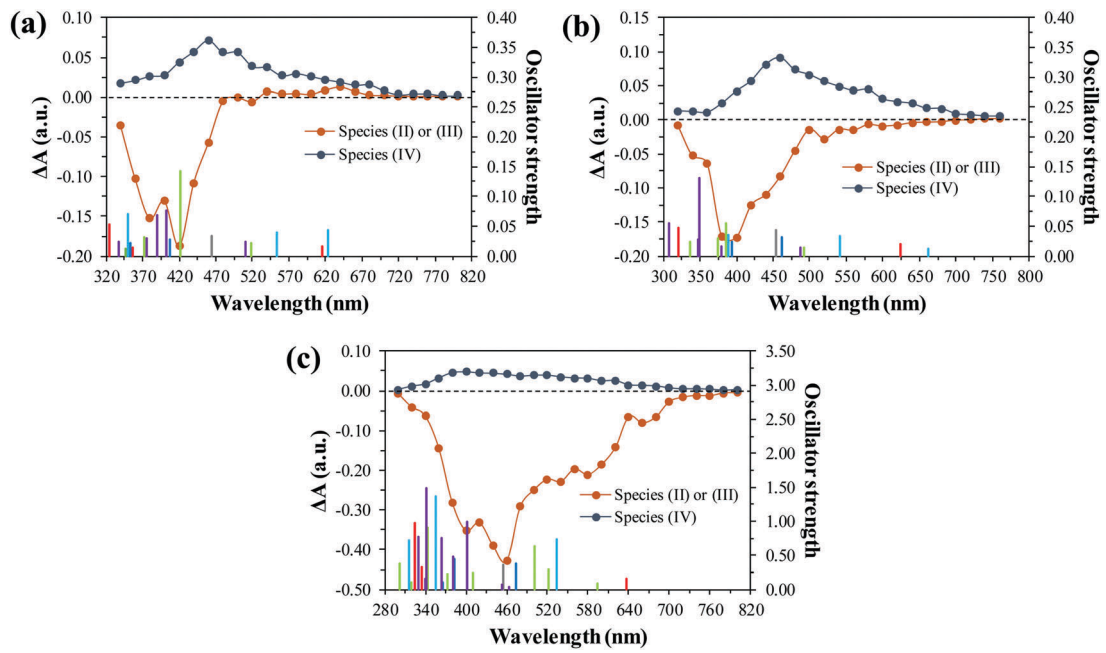

Fig. 4 Absorption spectra obtained from the kinetic profiles of the reactions of Fe^{3+} at pH = 3 with: (a) 4-*tert*-butylcatechol at $t = 32$ (t_{min}) and 372 ms (t_{max}), (b) catechol at $t = 28$ (t_{min}) and 388 ms (t_{max}), and (c) 3,4-dihydroxybenzonitrile at $t = 28$ (t_{min}) and 384 ms (t_{max}). The calculated oscillator strengths are also shown for: species II or IV (green), species III (purple), species V (blue), species VI (light blue), species VII (red), and species VIII (grey).

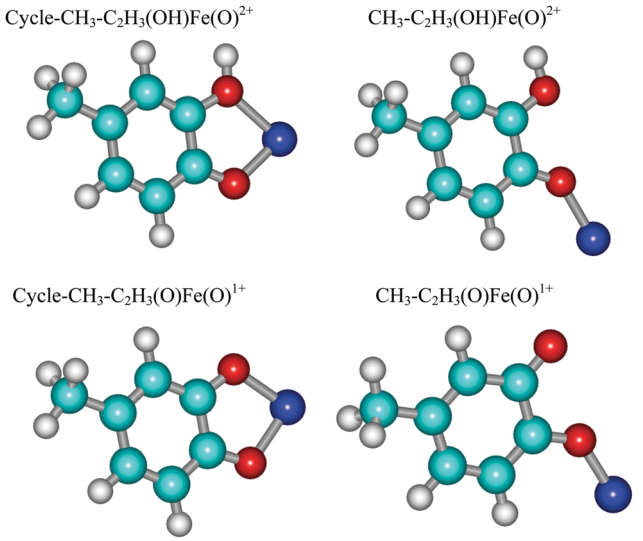

Fig. 5 Optimized geometries of the bidentate and monodentate complexes of Fe^{2+} and Fe^{3+} with 4-methylcatechol.

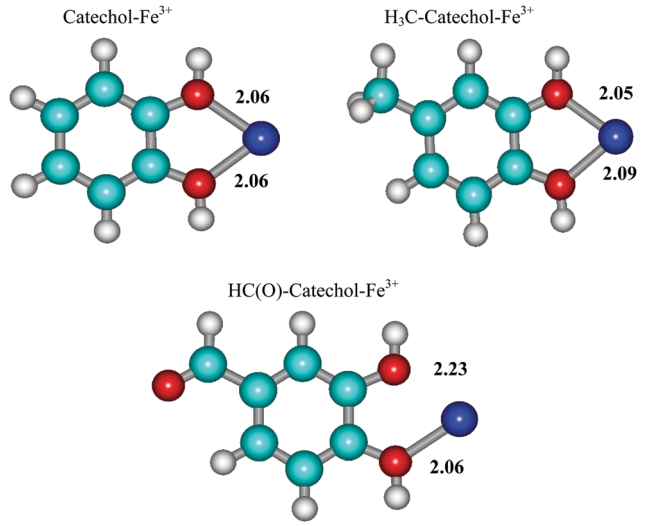

Fig. 6 Optimized geometries of the Fe^{3+} complexes. The distances are given in Å.

whereas the opposite is found for the Fe^{2+} complexes. Thus, it seems reasonable to propose the formation of an Fe^{3+} monodentate complex, which upon reduction yields a bidentate Fe^{2+} complex.

However, the previous calculations do not take into account that under our experimental conditions (pH = 3), since the pK_a of the first −OH group of these molecules is within the range 6–9,[33,34] both –OH groups of the catechol moiety should be protonated. Thus, calculations were also done for species I and II taking 3,4-dihydroxybenzaldehyde as an example of 1,2-DHB with EWS, 4-methylcatechol as representative of 1,2-DHB with EDS, and for the unsubstituted catechol. The optimized geometries of the Fe^{3+} complexes are shown in Fig. 6.

Note that for 3,4-dihydroxybenzaldehyde, the compound taken as example of 1,2-DHB with EWS, the monodentate is 6.1 kcal mol^{-1} more stable than the bidentate complex. In contrast, Table 1 shows that the bidentate complex of Fe^{3+} is more stable than the monodentate when one of the –OH groups is deprotonated. These results indicate that the relative stability of the Fe^{3+} complexes strongly depends on the protonation of the catechol −OH groups.

Energy calculations (Scheme 3a for catechol and 4-methylcatechol and Scheme 3b for 3,4-dihydroxybenzaldehyde) show that: (i) there is a stabilization of *ca.* 140–150 kcal mol^{-1} upon formation of the complexes between Fe^{3+} and 1,2-DHB, (ii) the more stable complex is cyclic for catechol and 4-methylcatechol, but open monodentate for 3,4-dihydroxybenzaldehyde, and (iii) there is an increase of ΔG° upon deprotonation of the complexes in all cases. From these results, it should be very unlikely that once the Fe^{3+} complex is formed the reactions go uphill about 100 kcal mol^{-1} to yield the deprotonated complexes, as proposed in the literature for catechol and its derivatives.[15,17] Thus, complexation should not occur before deprotonation and it would be feasible that a concerted mechanism takes place, *i.e.*, formation of the Fe–O bonds and proton loss occur in a single step without involving the participation of complex (I), in complete agreement with the stopped-flow data.

Table 1 Relative Gibbs free energies at 298 K (in kcal mol^{-1}) for different R-1,2-DHB–Fe complexes

R	Cycle-R-C_2H_3(OH)Fe^{III}(O)$^{2+}$-R-C_2H_3(OH)Fe^{III}(O)$^{2+}$	Cycle-R-C_2H_3(OH)Fe^{II}(O)$^{+}$-R-C_2H_3(OH)Fe^{II}(O)$^{+}$
–C(CH$_3$)$_3$	2.9	−12.0
–C$_2$H$_5$	10.9	−13.2
–CH$_3$	11.5	−23.2
–H	2.5	−23.4
–C(O)H	15.5	−11.3
–C(O)OH	7.6	−11.4
–CN	12.4	−12.4
–NO$_2$	14.1	−22.6

Our DFT data also show that bidentate deprotonated Fe^{2+} complexes are more stable than monodentate complexes. Thus, the second observed kinetic step in the stopped-flow experiments (electron transfer) should be accompanied by a cyclization process in the case of 1,2-DHB with EDS, as shown in Scheme 4.

The slowest observed kinetic step corresponds to deprotonation of the Fe^{2+} complex (Scheme 4).

DFT calculations were performed in order to obtain energetic information about possible final steps of the reaction. The oxidation of the deprotonated complex by the excess of Fe^{3+} leading to formation of quinones was considered as a possible end step. DFT calculations support the feasibility of this reaction route (see the calculated Gibbs energy for 4-methylcatechol and 3,4-dihydroxybenzaldehyde in Scheme 5).

4. Conclusion

The kinetics of the reaction of Fe^{3+} with 1,2-DHB is strongly dependent on the substituent. The absorbance changes could be well fitted to the sum of three exponential terms, these being the rate constants associated with the processes affected by the electron-withdrawing ability of the substituent. It was possible

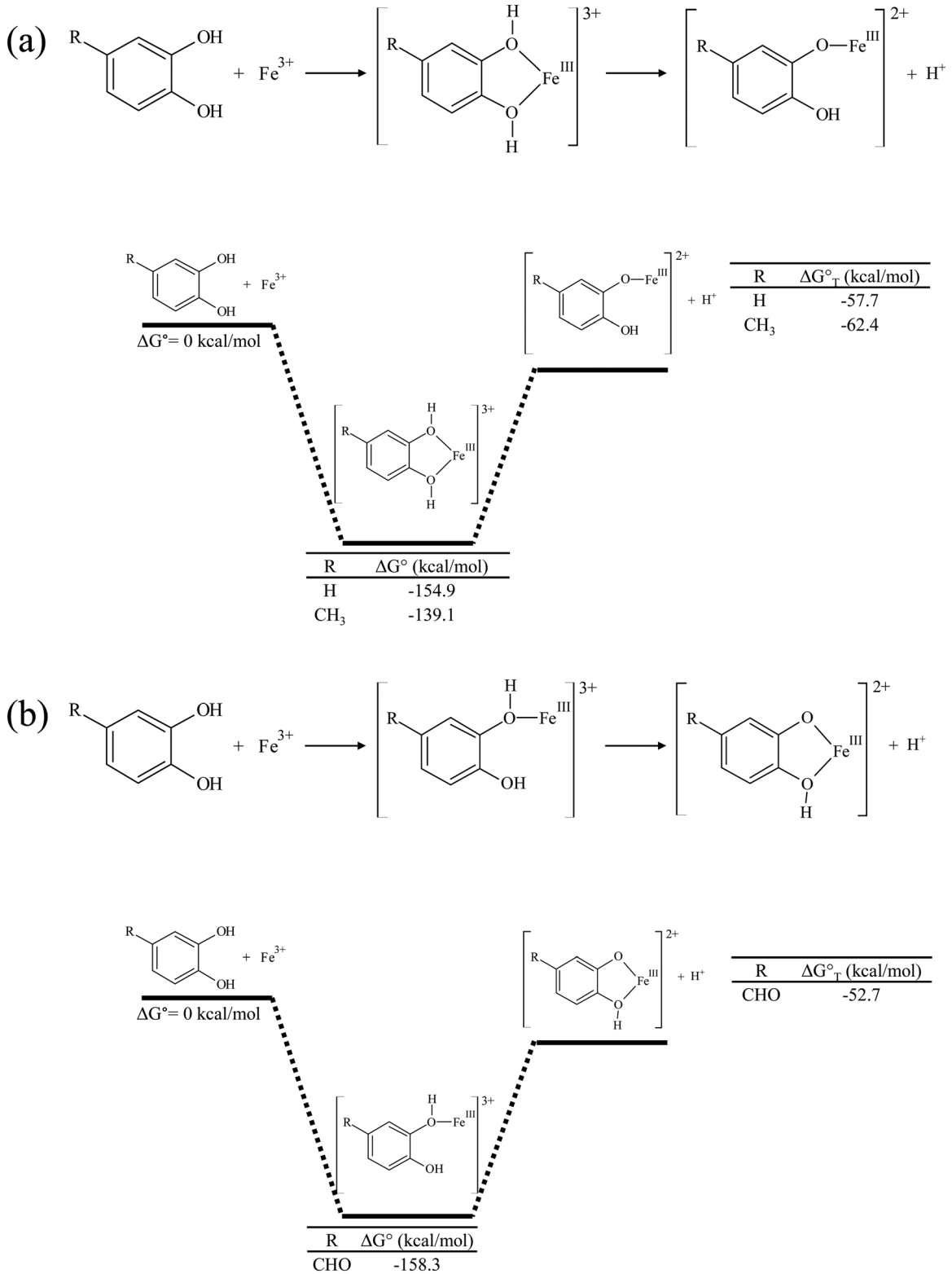

Scheme 3 Energy diagram for the complexation/deprotonation reaction of Fe^{3+} with: (a) catechol and 4-methylcatechol, (b) 3,4-dihydroxybenzaldehyde. This complex is monodentate for 3,4-dihydroxybenzaldehyde. The most stable species are only depicted in the scheme.

to obtain the absorption spectra of the deprotonated Fe^{3+} complexes, as well as those of the Fe^{2+} complexes formed by intramolecular charge transfer.

DFT calculations on mono- and bidentate species with different degrees of protonation helped us to evaluate their contribution to the reaction mixture.

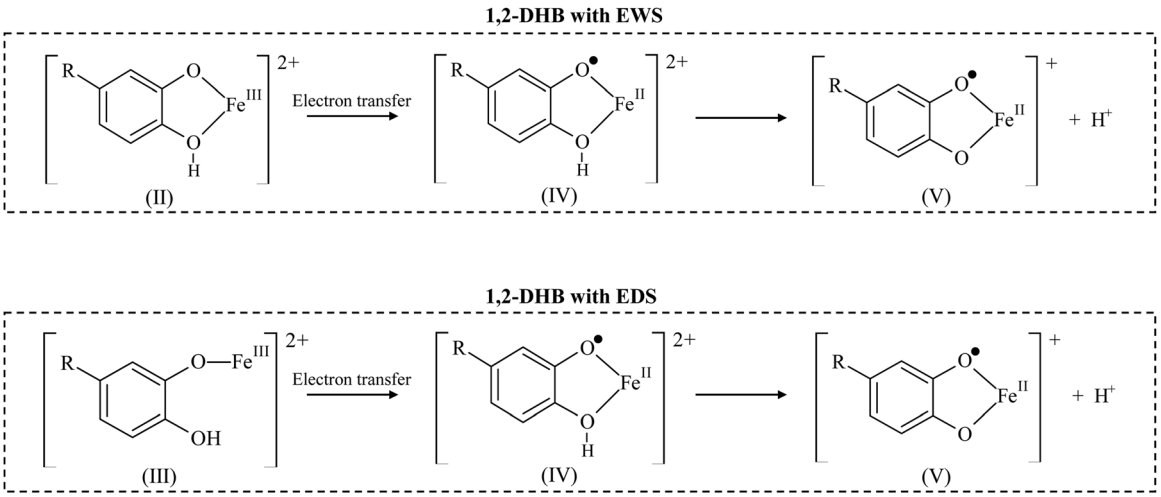

Scheme 4 Electron transfer and deprotonation steps according to the DFT results.

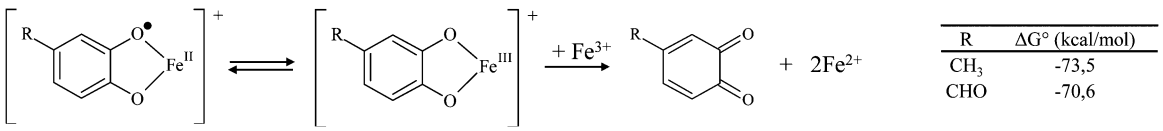

R	ΔG° (kcal/mol)
CH_3	-73,5
CHO	-70,6

Scheme 5 End step of the reaction of Fe^{3+} with the 1,2-dihydroxybenzenes in the presence of excess Fe^{3+}.

Energy calculations show that the more stable complex between Fe^{3+} and DHB is cyclic for catechol and 4-methylcatechol, but open monodentate for 3,4-dihydroxybenzaldehyde. These results indicate that the oxidation of catechol by Fe^{3+} should involve different intermediates depending on the substituent. Note that the participation of open monodentate complexes was not considered in the literature.[15,17,18] From the large increase in ΔG° upon deprotonation, it should be very unlikely for the reaction of species I to yield species III, as proposed in the literature for catechol and some of its derivatives.[15,17] Thus, we conclude from the experimental and theoretical data obtained here that formation of the Fe–O bonds and proton loss occurs in a single step.

Additionally, our DFT data also show that, since bidentate deprotonated Fe^{2+} complexes are more stable than monodentate complexes, the electron transfer process should be accompanied by a cyclization process in the case of 1,2-DHB with EDS.

Conflicts of interest

There are no conflicts to declare.

Acknowledgements

The financial support for this work was provided by FONDECYT (Grant No. 1160100) and CONICYT/FONDAP (Grant No. 15130015). Pablo Salgado wishes to acknowledge the CONICYT PhD fellowship (Grant # 21120966), REDOC fellowship and UDT-CCTE fellowship (Grant # PFT-072). The authors thank the Consejo Nacional de Investigaciones Científicas y Técnicas CONICET (PIP 2012-134) and the Agencia Nacional de Promoción Científica y Tecnológica (PICT 2012-478 and PICT 2012-1817). C. C. is a research member of CONICET. D. O. M. is a research member of Comisión de Investigaciones Científicas de la Provincia de Buenos Aires (Argentina).

References

1 C. E. Lankford and B. R. Byers, *Crit. Rev. Microbiol.*, 1973, **2**, 273–331.
2 V. Arantes, A. M. F. Milagres, T. R. Filley and B. Goodell, *J. Ind. Microbiol. Biotechnol.*, 2011, **38**, 541–555.
3 B. Goodell, J. Jellison, J. Liu, G. Daniel, A. Paszczynski, F. Fekete, S. Krishnamurthy, L. Jun and G. Xu, *J. Biotechnol.*, 1997, **53**, 133–162.
4 S. M. Hyde and P. M. Wood, *Microbiology*, 1997, **143**, 259–266.
5 J. W. Koenigs, *Arch. Microbiol.*, 1974, **99**, 129–145.
6 E. Espejo and E. Agosin, *Appl. Environ. Microbiol.*, 1991, **57**, 1980–1986.
7 Y. Qian, B. Goodell and C. C. Felix, *Chemosphere*, 2002, **48**, 21–28.
8 Y. Zhu, L. Zhuang, B. Goodell, J. Cao and J. Mahaney, *Int. Biodeterior. Biodegrad.*, 2016, **109**, 185–190.
9 M. Bisaglia, R. Filograna, M. Beltramini and L. Bubacco, *Ageing Res. Rev.*, 2014, **13**, 107–114.
10 A. D. Surowka, P. Wrobel, D. Adamek, E. Radwanska and M. Szczerbowska-Boruchowska, *Metallomics*, 2015, **7**, 1522–1531.
11 K. Jomova and M. Valko, *Toxicology*, 2011, **283**, 65–87.

12 E. Mentasti, E. Pelizzetti and G. Saini, *J. Inorg. Nucl. Chem.*, 1976, **38**, 785–788.
13 J. Xu and R. B. Jordan, *Inorg. Chem.*, 1988, **27**, 4563–4566.
14 A. Aguiar, A. Ferraz, D. Contreras and J. Rodríguez, *Quim. Nova*, 2007, **30**, 623.
15 V. Kristinová, R. Mozuraityte, I. Storrø and T. Rustad, *J. Agric. Food Chem.*, 2009, **57**, 10377–10385.
16 W. Linert, R. F. Jameson and E. Herlinger, *Inorg. Chim. Acta*, 1991, **187**, 239–247.
17 R. C. Hider, B. Howlin, J. R. Miller, A. R. Mohd-Nor and J. Silver, *Inorg. Chim. Acta*, 1983, **80**, 51–56.
18 M. J. Hynes and M. n. O'Coinceanainn, *J. Inorg. Biochem.*, 2004, **98**, 1457–1464.
19 N. R. Perron and J. L. Brumaghim, *Cell Biochem. Biophys.*, 2009, **53**, 75–100.
20 L. K. Charkoudian and K. J. Franz, *Inorg. Chem.*, 2006, **45**, 3657–3664.
21 H. Powell and M. Taylor, *Aust. J. Chem.*, 1982, **35**, 739–756.
22 R. F. Jameson and M. F. Wilson, *J. Chem. Soc., Dalton Trans.*, 1972, 2617–2621, DOI: 10.1039/DT9720002617.
23 V. M. Nurchi, T. Pivetta, J. I. Lachowicz and G. Crisponi, *J. Inorg. Biochem.*, 2009, **103**, 227–236.
24 A. M. Berkovic, M. C. Gonzalez, N. Russo, M. del Carmen Michelini, R. P. Diez and D. O. Mártire, *J. Phys. Chem. A*, 2010, **114**, 12845–12850.
25 A. J. Cohen and N. C. Handy, *Mol. Phys.*, 2001, **99**, 607–615.
26 W.-M. Hoe, A. J. Cohen and N. C. Handy, *Chem. Phys. Lett.*, 2001, **341**, 319–328.
27 C. Lee, W. Yang and R. G. Parr, *Phys. Rev. B: Condens. Matter Mater. Phys.*, 1988, **37**, 785–789.
28 V. Barone and M. Cossi, *J. Phys. Chem. A*, 1998, **102**, 1995–2001.
29 M. J. Frisch, G. W. Trucks, H. B. Schlegel, G. E. Scuseria, M. A. Robb, J. R. Cheeseman, G. Scalmani, V. Barone, B. Mennucci, G. A. Petersson, H. Nakatsuji, M. Caricato, X. Li, H. P. Hratchian, A. F. Izmaylov, J. Bloino, G. Zheng, J. L. M. Sonnenberg, Hada, M. Ehara, K. Toyota, R. Fukuda, J. Hasegawa, M. Ishida, T. Nakajima, Y. Honda, O. Kitao, H. Nakai, T. Vreven, J. A. Montgomery Jr., J. E. Peralta, F. Ogliaro, M. Bearpark, J. J. Heyd, E. Brothers, K. N. Kudin, V. N. Staroverov, R. Kobayashi, J. Normand, K. Raghavachari, A. Rendell, J. C. Burant, S. S. Iyengar, J. Tomasi, M. Cossi, N. J. Rega Millam, M. Klene, J. E. Knox, J. B. Cross, V. Bakken, C. Adamo, J. Jaramillo, R. E. Gomperts, O. Stratmann, A. J. Yazyev, R. Austin, C. Cammi, J. W. Pomelli, R. Ochterski, R. L. Martin, K. Morokuma, V. G. Zakrzewski, G. A. Voth, P. Salvador, J. J. Dannenberg, S. Dapprich, A. D. Daniels, O. Farkas, J. B. Foresman, J. V. Ortiz, J. Cioslowski and D. J. Fox, *Gaussian 09, Revision A 02*, Gaussian Inc., Wallingford, CT, 2009.
30 C. Hansch, A. Leo and R. W. Taft, *Chem. Rev.*, 1991, **91**, 165–195.
31 J. A. Peres, J. R. Domínguez and J. Beltran-Heredia, *Desalination*, 2010, **252**, 167–171.
32 T. Ishida, H. Tanaka and K. Horiike, *J. Biochem.*, 2004, **135**, 721–730.
33 R. Aydin, Ö. Ulviye and N. Türkel, *Turk. J. Chem.*, 1997, **21**, 428–436.
34 R. Pizer and L. Babcock, *Inorg. Chem.*, 1977, **16**, 1677–1681.